Materials Science and Engineering, A188 (1994) 103–112

Delamination of beams under transverse shear and bending

T. J. Lu, Z. C. Xia and J. W. Hutchinson

Division of Applied Sciences, Harvard University, Cambridge, MA 02138 (USA)

(Received October 4, 1993)

Abstract

Two delamination problems are studied: a straight beam of rectilinearly orthotropic material under transverse loading and a curved beam (or C-specimen) with cylindrical material anisotropy under pure bending. Results are presented for each problem for the dependence on the crack length of both the energy release rate and a measure of the relative amount of mode II to mode I. The number of nondimensional parameters in the problems is fairly large, including two dimensionless elasticity parameters. Considerable simplification of the parametric dependence in the straight beam problem is achieved using an orthotropic rescaling technique due to Suo. Asymptotic solutions based on elastic beam theory are also presented. A by-product of the present analysis is the finding that frictionless contact of the crack faces near one of the crack tips has little effect on the other tip, even in the case when the size of the contact zone is large relative to the length of the crack.

1. Introduction

Delamination, a splitting apart into layers, is believed to be one of the dominant failure modes in most layered materials, such as wood and fiber reinforced composites. The problem of delamination is important to composite design because it impairs not only the strength but also leads to a substantial loss of stiffness of structural components. Delamination specimen calibrations are badly needed in composite design in order to determine delamination toughness parameters by experiment. They also enable assessment of critical load conditions at which delamination failures occur in actual components, hence establishing a data base for delamination under a variety of complex loadings.

Two beam-like geometries, each weakened by a preexisting delamination crack, are studied here using the finite element method, in conjunction with some other analytical tools. Depicted in Fig. 1(a) is the orthotropic straight beam under transverse load. The axes of orthotropy are aligned with beam, which contains a crack of length $2a$ parallel to the beam direction. The beam, which is long compared to the crack length, is clamped at the left end and the downward force P per unit width in the x_3-direction is applied at the other end. In Fig. 2(a), a curved circular beam has cylindrically orthotropic material properties. It is bent by a moment M per unit width (in x_3-direction) applied at the ends. A circular crack of length $2a$ is introduced. In both of these problems, material homogeneity and linearly elastic behavior are assumed. Frictionless contact of crack surfaces will be accounted for whenever applicable.

Conceptual developments related to the two problems are presented first to provide the relevant background. These are followed by a discussion of orthotropy rescaling as applied to the straight beam. This method helps to address the complication presented by the relatively large number of geometric and

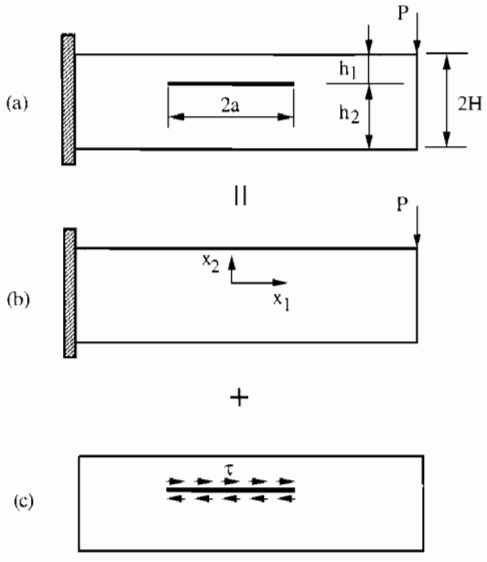

Fig. 1. Conventions and superposition scheme for straight beam specimen.

0921-5093/94/$7.00
SSDI 0921-5093(93)09531-Z

material parameters involved in the solutions to these problems. Elastic beam theory is invoked in due course to generate approximate solutions in limiting cases for each problem. These serve as an independent check of the accuracy of the full numerical solutions from the finite element models.

2. Preliminaries related to material orthotropy

Following Suo [1], introduce two in-plane dimensionless elastic parameters

$$\lambda=\frac{E_2}{E_1}, \quad \rho=\frac{(E_1E_2)^{1/2}}{2G_{12}}-(\nu_{12}\nu_{21})^{1/2} \tag{1}$$

Assuming plane stress ($\sigma_{33}=0$), which prevails throughout the present analysis, the elastic constants are defined in terms of stress–strain relations which are written in axes aligned with the local axes of orthotropy

$$\begin{aligned}
\varepsilon_{11}&=\frac{1}{E_1}\sigma_{11}-\frac{\nu_{21}}{E_2}\sigma_{22}-\frac{\nu_{31}}{E_3}\sigma_{33}\\
\varepsilon_{22}&=-\frac{\nu_{12}}{E_1}\sigma_{11}+\frac{1}{E_2}\sigma_{22}-\frac{\nu_{32}}{E_3}\sigma_{33}\\
\varepsilon_{33}&=-\frac{\nu_{13}}{E_1}\sigma_{11}-\frac{\nu_{23}}{E_2}\sigma_{22}+\frac{1}{E_3}\sigma_{33}\\
\sigma_{12}&=\frac{1}{2G_{12}}\sigma_{12}
\end{aligned} \tag{2}$$

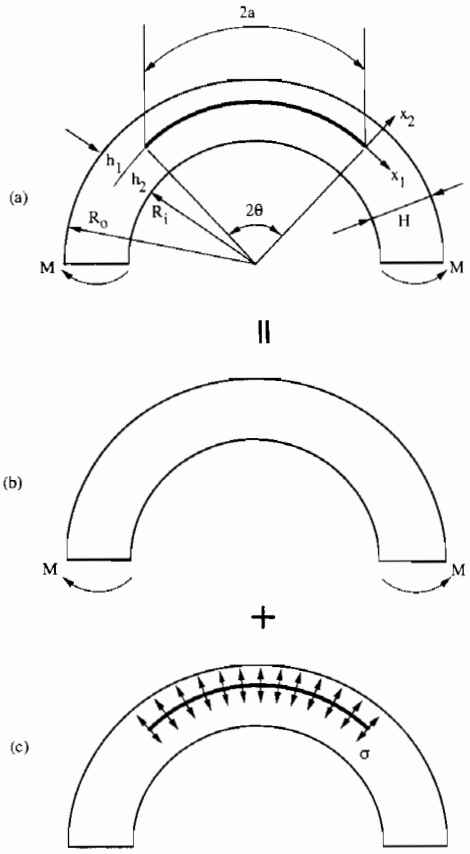

Fig. 2. Conventions and superposition scheme for curved beam specimen.

In what follows, the crack plane at the tip is aligned with the local x_1-axis (Fig. 1). For plane strain problems, the definition of λ and ρ remains unchanged except that the elastic constants need to be replaced respectively by the following primed quantities:

$$E_1'=E_1/(1-\nu_{13}\nu_{31}), \quad E_2'=E_2/(1-\nu_{23}\nu_{32})$$
$$\nu_{12}'=(\nu_{12}+\nu_{13}\nu_{32})/(1-\nu_{13}\nu_{31}),$$
$$\nu_{21}'=(\nu_{21}+\nu_{23}\nu_{31})/(1-\nu_{23}\nu_{32})$$

There is, however, no need to change the transverse shear modulus G_{12}. This replacement carries through all the solutions in the body of the text if plane strain holds.

The beauty of the choice of λ and ρ stems from its ability to reduce a two-dimensional problem, otherwise depending on three nondimensional parameters for rectilinearly orthotropic materials, to a one-parameter problem for materials with cubic in-plane symmetry, *i.e.* $\lambda=1$. A transversely isotropic (or in-plane isotropic) material with respect to the x_3-axis corresponds to $\lambda=\rho=1$. Positive definiteness of the strain energy density requires $\lambda>0$ and $-1<\rho<\infty$. Practical ranges of λ and ρ for representative woods and composites are $0<\rho<5$ and $0<\lambda<20$ [1].

The opening and sliding stresses a short distance r ahead of the crack tip in an orthotropic solid are still given by the well-known inverse square-root singular fields for isotropic materials [2]

$$\sigma_{22}=K_I(2\pi r)^{-1/2} \qquad \sigma_{12}=K_{II}(2\pi r)^{-1/2} \tag{3}$$

with K_I and K_{II} representing the standard mode I and mode II stress intensity factors. The relative displacements of the crack faces behind the tip associated with the singular fields (eqn. (3)) are

$$(\delta_2,\,\delta_1)=\frac{8n}{(E_1E_2)^{1/2}}\left(\frac{r}{2\pi}\right)^{1/2}(\lambda^{-1/4}K_I,\,\lambda^{1/4}K_{II}) \tag{4}$$

where $n=[(1+\rho)/2]^{1/2}$. For a self-similar increment of crack advance, the energy release rate can be expressed as

$$G=G_I+G_{II} \tag{5}$$

where, in accordance with the composite literature,

$$(G_I, G_{II}) = \frac{n}{(E_1 E_2)^{1/2}} (\lambda^{-1/4} K_I^2, \lambda^{1/4} K_{II}^2) \tag{6}$$

The measure of the relative amount of mode II to mode I is defined by the phase angle

$$\psi = \tan^{-1}(K_{II}/K_I) \tag{7a}$$

or, equivalently, by

$$\psi = \tan^{-1}[\lambda^{-1/4}(G_{II}/G_I)^{1/2}] \tag{7b}$$

The two quantities G and ψ are used to characterize conditions for a mixed mode delamination crack to advance according to [3–6]

$$G = G_c(\psi) \tag{8}$$

where $G_c(\psi)$ is the mode-dependent delamination toughness.

3. Straight beam under transverse shear load

To see how the method of orthotropy rescaling developed in ref. 1 can be used to extract the λ dependence of the solution explicitly, denote the Airy stress function by $\phi(x_1, x_2)$ such that the compatibility equation for rectilinearly anisotropic material is obtained as [7]

$$\frac{\partial^4 \phi}{\partial x_1^4} + 2\rho\lambda^{1/2} \frac{\partial^4 \phi}{\partial x_1^2 \partial x_2^2} + \lambda \frac{\partial^4 \phi}{\partial x_2^4} = 0 \tag{9}$$

Rescale the x_1-axis with the elastic parameter λ according to

$$\eta_1 = \lambda^{1/4} x_1 \tag{10}$$

This reduces eqn. (9) to

$$\frac{\partial^4 \phi}{\partial \eta_1^4} + 2\rho \frac{\partial^4 \phi}{\partial \eta_1^2 \partial x_2^2} + \frac{\partial^4 \phi}{\partial x_2^4} = 0 \tag{11}$$

Now the governing equation does not depend on λ explicitly and the traction boundary conditions are changed accordingly to

$$\sigma_{11} = \frac{\partial^2 \phi}{\partial x_2^2}, \quad \lambda^{-1/2}\sigma_{22} = \frac{\partial^2 \phi}{\partial \eta_1^2}, \quad \lambda^{-1/4}\sigma_{12} = -\frac{\partial^2 \phi}{\partial \eta_1 \partial x_2} \tag{12}$$

An inspection of eqns. (3) and (12) reveals that the following combinations are independent of λ:

$$\lambda^{-3/8} K_I \sim (2\pi\eta_1)^{1/2} \frac{\partial^2 \phi}{\partial \eta_1^2}$$
$$\lambda^{-1/8} K_{II} \sim -(2\pi\eta_1)^{1/2} \frac{\partial^2 \phi}{\partial \eta_1 \partial x_2} \tag{13}$$

Define an auxiliary phase angle $\omega \equiv \tan^{-1}(\lambda^{1/4} K_{II}/K_I)$ related to ψ by

$$\tan\psi = \lambda^{-1/4} \tan\omega \tag{14}$$

Noting that $\delta_1/\delta_2 = \lambda^{1/2} K_{II}/K_I$, ω can be rewritten as

$$\tan\omega = \lambda^{-1/4} \left(\lambda^{1/2} \frac{K_{II}}{K_I}\right) = \lambda^{-1/4} \frac{\delta_1}{\delta_2} \tag{15}$$

Since ω is independent of λ, one can always make the choice $\lambda = 1$, which coincides with cubic in-plane material symmetry.

Dimensional analysis guided by the orthotropy rescaling illustrated above dictates that the paramcters defined in Fig. 1 must combine according to

$$\frac{\lambda^{1/4} E_1 G}{\tau^2 a} = F_I \left(\eta, \lambda^{1/4} \frac{a}{H}, \rho\right) \tag{16a}$$

and

$$\psi = \Psi_I \left(\eta, \lambda^{1/4} \frac{a}{H}, \rho\right) \tag{16b}$$

where $\eta = h_1/h_2$ and $h_1 + h_2 = 2H$. It is to be understood that ψ given above applies to the right-hand tip and is defined for a positive τ. With the material parameter λ and the geometrical parameter a/H combined due to orthotropy rescaling, F_I and Ψ_I are functions of three dimensionless variables instead of four. As schematically depicted in Fig. 1, the stress intensity factors and the relative crack face displacements are identical to those of the problem in Fig. 1(c) if

$$\tau = \frac{3P}{4\lambda^{1/4} H} \left[1 - \left(\frac{y}{H}\right)^2\right] \tag{17}$$

All the solutions reported below are therefore for the reduced problem of Fig. 1(c).

For very short cracks, $K_{II} = \tau\sqrt{(\pi a)}$ which, in combination with eqn. (6), leads to

$$F_I = \pi \sqrt{\frac{1+\rho}{2}}, \quad \Psi_I \cong 90° \tag{18}$$

For short to intermediate length cracks in infinitely long beams, and for $\eta = 1$, the dimensionless function F_I has been obtained by Fourier transform methods [8–9] giving:

$$F_1 \approx \frac{3[1.13s+0.285(1-s)]^2}{s(1-s)}\sqrt{\frac{1+\rho}{2}}, \quad \Psi_1 \equiv 90° \quad (19)$$

with

$$s = \frac{1}{1+\lambda^{-1/4}H/a} \quad (20)$$

Equation (19) is valid only for $0.4 < s < 1.0$. A representation of the solution for $0 < s < 0.4$ can be found in refs. 8 and 9. For very long cracks, the mathematical problem can be solved approximately using a simple beam analysis with the result $K_{II} = 2\tau a/\sqrt{H}$ or

$$F_1 = \frac{4a}{H}\sqrt{\frac{1+\rho}{2}}, \quad \Psi_1 \cong 90° \quad (21)$$

In principle, one could use Fourier transform methods to solve the straight beam problem for arbitrary η. We have found it more straightforward to generate results using the finite element method, especially since it will carry over to the curved beam problem. The finite element code, ABAQUS, has been used to determine energy release rates and the corresponding phase angles for a large variety of combinations of material parameters and geometrical factors. Every attempt has been made to present the results in as comprehensive a manner as possible, given the number of parameters involved.

Since there is no general symmetry in the problem, the whole beam was modeled with eight-noded quadrilateral plane stress elements. Quarter-point elements were used to simulate the singular behavior of stress and strain fields in the immediate adjacency of each crack tip. The energy release rate is obtained by numerical evaluation of the J-integral. By virtue of eqns. (4) and (7), the values of ψ are obtained directly from crack face displacements δ_2 and δ_1 behind the crack tip.

Convergence studies for G and ψ were performed for both geometries, and the numerical solutions were compared with the available analytic solutions for isotropic materials. These studies were used to establish the mesh used in the calculations. A special program was developed to generate all requisite meshes for each problem.

For $\eta = 1$, the crack is in pure mode II. The calculated dimensionless energy release rate, F_1, is plotted in Fig. 3(a) *vs.* the crack-length-to-beam-thickness ratio a/H contracted by the orthotropy factor $\lambda^{1/4}$. In the numerical model, to minimize possible end effects, the beam length was taken to be 20 times that of the crack length. Values generated by the numerical model are shown as solid points in the figures, while the curves are simply straight line interpolations of the numerical

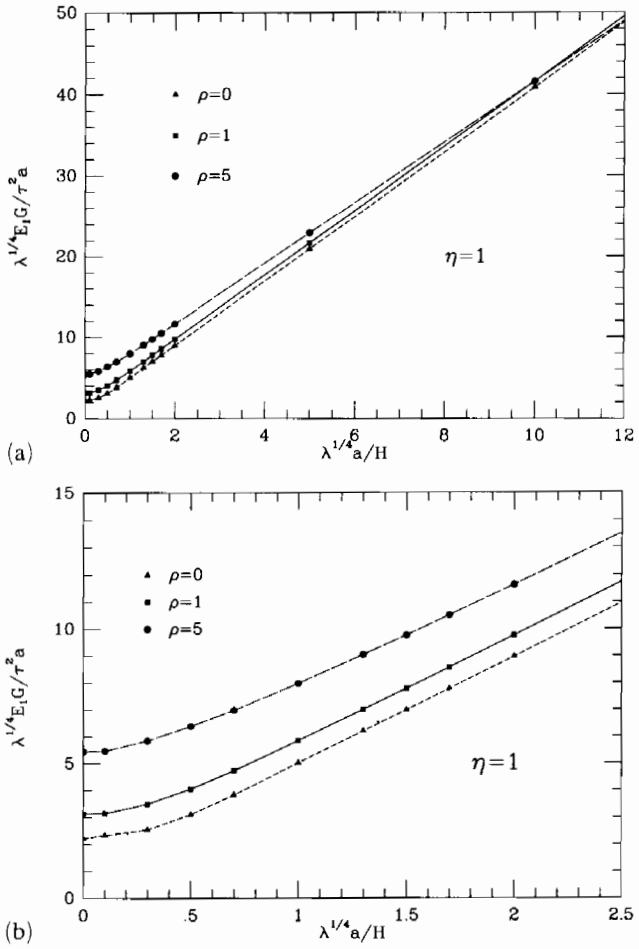

Fig. 3. (a) The normalized energy release rate as a function of $\lambda^{1/4}a/H$ for $\eta = 1$. (b) The enlarged view in the transition range.

values. One feature of the results is that the normalized energy release rate increases continuously as the value of the dimensionless parameter ρ is raised from 0 to 5; this is most pronounced for small values of $\lambda^{1/4}a/H$ (Fig. 3(b)). Observe that the calculated F_1 value approaches the short-crack solution (eqn. (18)) asymptotically as $\lambda^{1/4}a/H \to 0$. For larger $\lambda^{1/4}a/H$ values, it is noteworthy that all curves straighten. The slope of the line for $\rho = 1$ (and also for $\rho = 0$) is hardly distinguishable from 4, which is the result from the elastic beam analysis (*cf.* eqn. (21)). It is interesting to note that the curve for $\rho = 5$ falls below that for $\rho = 1$ when $\lambda^{1/4}a/H$ exceeds 9. Similar trends are observed for mixed-mode situations ($\eta \neq 1$). An obvious explanation for this trend has not been discovered.

When $\eta < 1$ (or equivalently for $\eta > 1$), mixed-mode behavior sets in such that one needs to account for the contact of crack faces near one of the crack tips. Frictionless contact was assumed and an iteration method was adopted to identify the contact region. A contact region of about 1/3 of the total crack length was

assumed in the first iteration. In subsequent iterations, the choice of contact region was checked against the requirements that the normal traction in the region be compressive and that the crack be open outside the region. The contact region was adjusted accordingly. The iteration process was continued until consistency was finally reached. This proves to be a viable method, at least for the present problems, since the process converges rapidly requiring only four to five steps to achieve an accuracy within 1%. For the case of $\eta = 1/3$ and $\rho = 1$ the influence of crack face contact at the left crack tip on energy release rate and phase angle at the right crack tip is shown in Fig. 4 as curves of normalized G and ψ against $\lambda^{1/4}a/H$. In all cases investigated here, crack face contact has a minor effect on the quantities of interest. This is evident in Fig. 4(a), where the energy release rate, computed with and without contact, are compared. The small effect on G and ψ occurs even though the size of the contact zone (which increases continuously as the value of $\lambda^{1/4}a/H$ is increased) may make up more than 1/2 of the total crack length in its extreme. Similarly good agreement was obtained for other combinations of η and ρ which are omitted here for the sake of brevity. A similar conclusion was reached by Liechti and Chai [5] in connection with their development of a mixed mode, bi-material test specimen. The effect of crack face contact has therefore been neglected in carrying out calculations given in the remainder of this report. It is worthwhile mentioning, however, that since frictionless contact was assumed in the calculations just described, the results reported here may not apply to situations where friction is no longer negligible.

The results for $\eta = 0.2$ and $\eta = 0.5$ are separately collected in Figs. 5 and 6, in the region $\lambda^{1/4}a/H \leq 2.5$, as this is the range of most practical concern. It is also in this region that the elastic beam analysis fails to give accurate results. A direct comparison of Figs. 5(a) and 6(a) with Fig. 3(a) reveals that the dimensionless elasticity parameter ρ affects the energy release rate in essentially the same way for all the mode mixities exhibited at the crack tip. For short cracks the influence of the geometrical factor η on F_1 is small. However, since the crack tip releases less energy for longer cracks when the crack is near the free surface, F_2 becomes smaller when η decreases. Intuitively one expects that the relative amount of shear to opening will be reduced as η decreases, and this is indeed

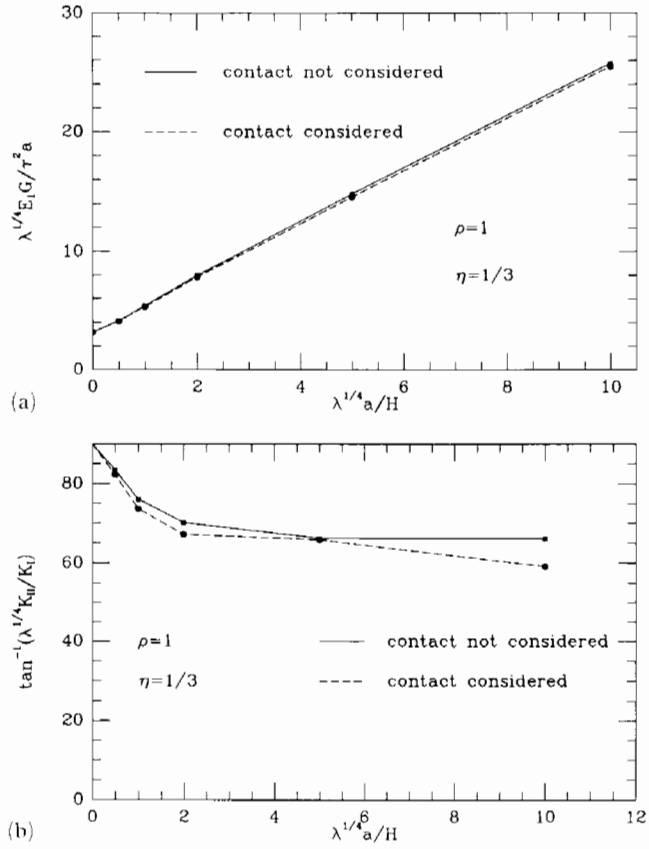

Fig. 4. The influence of crack face contact on (a) energy release rate, and (b) phase angle.

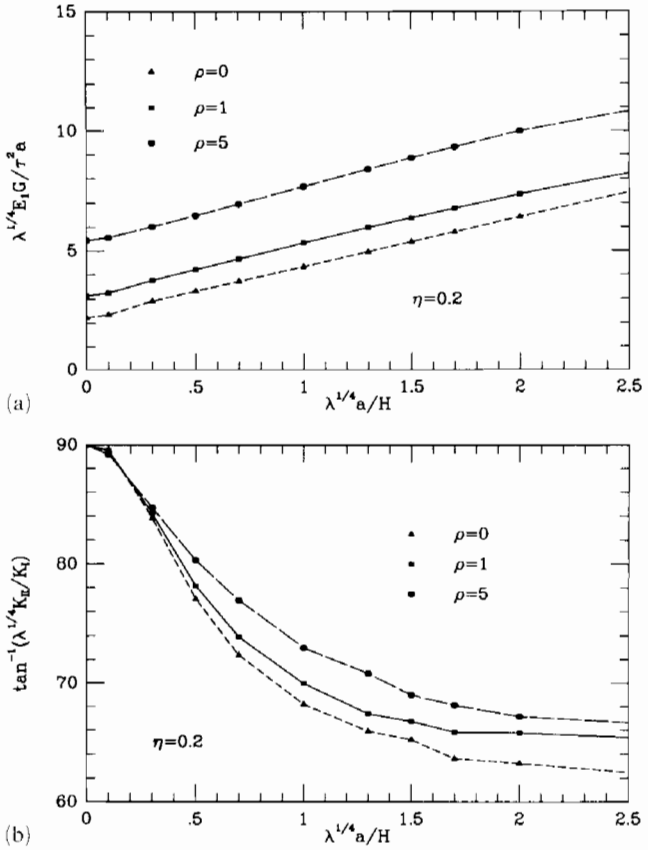

Fig. 5. The ρ-dependence of (a) energy release rate, and (b) phase angle for $\eta = 0.2$.

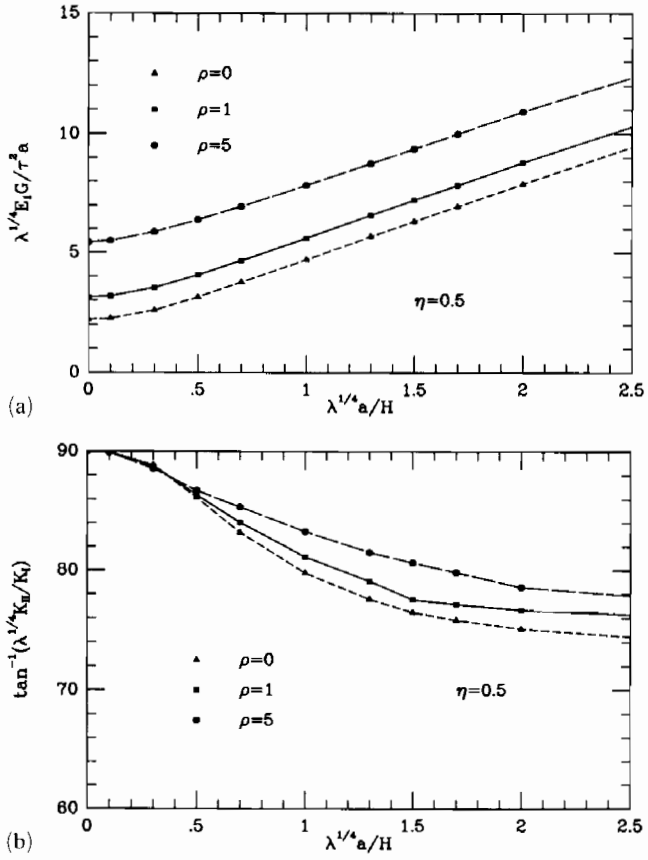

Fig. 6. The ρ-dependence of (a) energy release rate, and (b) phase angle for $\eta = 0.5$.

verified by the ψ *vs.* $\lambda^{1/4}a/H$ curves illustrated in Figs. 5(b) and 6(b). In passing, note also that ψ attains a "steady state" when $\lambda^{1/4}a/H$ approximately equals 2 which may be taken as the size of the transitional zone linking the results for the very short cracks to the longer cracks which can be adequately described by a beam theory approach.

4. Curved beam under pure bending

A curved beam under pure bending in the sense shown in Fig. 2(b) develops a tensile radial stress component. For the case of cylindrical material anisotropy, this stress σ acting normal to the prospective crack faces is related to the bending moment M by eqn. (A-6) in the Appendix. This solution is a function of λ but not ρ. The uncracked beam in Fig. 2(b) exhibits no stress singularity so that the problems in Figs. 2(a) and 2(c) have the same stress intensity factors. On the other hand, as the governing equation (eqn. (A-2)) for the cracked curved beam clearly shows, orthotropy rescaling cannot be exploited for the cylindrical geometry, and, therefore, the effect of both material parameters λ and ρ must be separately investigated. Or, formally, the normalized energy release rate and the mode mixity should take the form

$$\frac{E_1 H^3 G}{M^2} = F_2\left(\eta, \frac{a}{H}, \frac{R_i}{R_o}, \lambda, \rho\right)$$
$$\psi = \Psi_2\left(\eta, \frac{a}{H}, \frac{R_i}{R_o}, \lambda, \rho\right) \tag{22}$$

where R_i and R_o denote inner and outer radii of the beam respectively, $\eta = h_1/h_2$ and $h_1 + h_2 = H$ (Fig. 2). As remarked on earlier, the parameter set for this problem is fairly large.

For very short cracks, the crack is approximately in pure mode I with $K_I = \sigma\sqrt{(\pi a)}$. A companion solution to that of eqn. (18) is thus obtained as

$$\frac{\lambda^{3/4} E_1 G}{\sigma^2 a} = \pi\sqrt{\frac{1+\rho}{2}} \tag{23}$$

or, in terms of the bending moment M,

$$\frac{E_1 H^3 G}{M^2} = \pi\lambda^{-3/4}\left(\frac{a}{H}\right)\left(\frac{\sigma H^2}{M}\right)^2\sqrt{\frac{1+\rho}{2}} \tag{24}$$

As a first approximation and also as a guide for subsequent finite element method (FEM) calculations, the dimensionless functions F_2 and Ψ_2 were evaluated using an elastic curved beam analysis along lines which have been popular in the composite materials community [10, 11]. The core of this approach is to compute the elastic energy per unit length stored in the two curved beams separated by the crack far behind the crack tip. Since only the elastic modulus in the direction of the local beam axis is involved in the analysis, the results apply to the most general cylindrically orthotropic materials considered here. The approach, which is similar to that used for straight cracked beams, uses the curved beam theory of ref. 12 with the coupling between the bending and stretching neglected in the constitutive law for the beam. In the interests of brevity, details of this analysis are not recorded here. For the thin curved beam analysis, the roles of h_1 and h_2 may be interchanged. Figure 7 depicts F_1 as a function of the angle θ subtended by half of the crack length for $R_i/R_o = 4/5$, $2/3$ and $\eta < 1$. When θ exceeds a certain value, θ_s, the crack extension behavior approaches a steady state. As seen in Fig. 7, θ_s increases monotonically with increases in the magnitudes of η or R_i/R_o.

A finite element model similar to the one discussed in the last section was used to solve the mechanics problem in Fig. 2(c). The finite element discretization was made only for one half of the specimen due to the

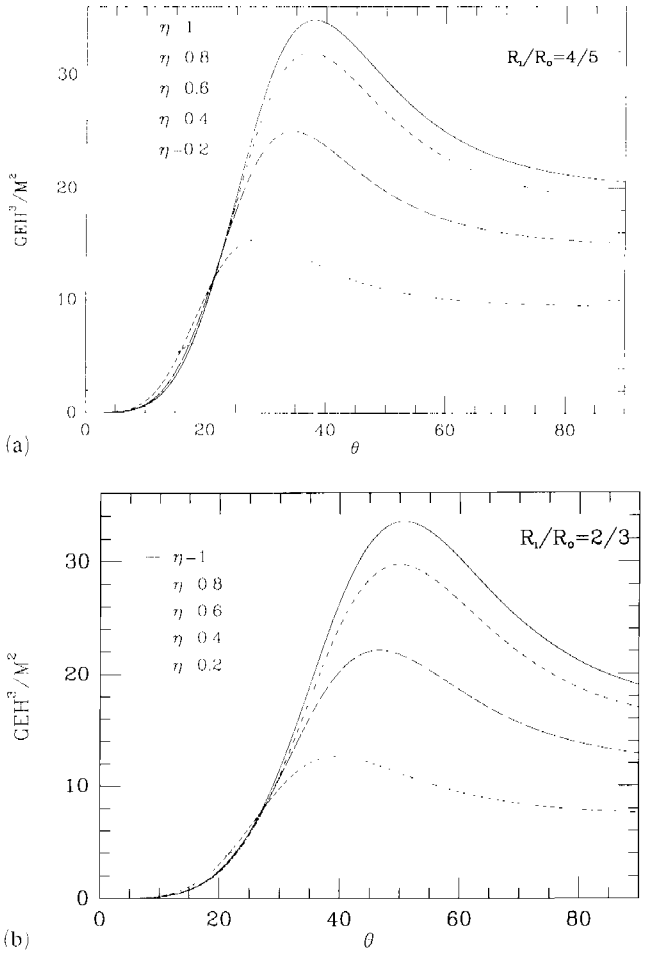

Fig. 7. Nondimensional energy release rate for delamination of the curved beam in bending from elastic curved beam theory: (a) $R_i/R_o = 4/5$, and (b) $R_i/R_o = 2/3$.

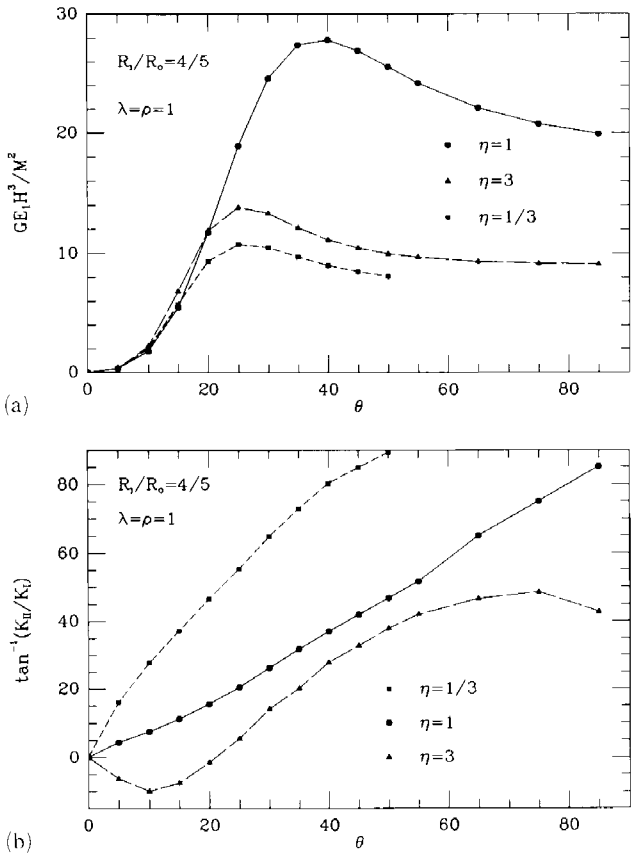

Fig. 8. The η-dependence of (a) energy release rate, and (b) phase angle for $R_i/R_o = 4/5$ and $\lambda = \rho = 1$.

symmetry of the problem, with a total of approximately 600 isoparametric elements and 1000 nodes. In general, the finite element mesh was arranged in such a way that it accommodated both the high stress gradient region close to the crack tip and the large dimensions of the remainder of the specimen.

To use the J-integral to extract G, an approximation was made by replacing a tiny section of the curved crack at the tip by a straight line segment. A convergence study was conducted to ensure the high accuracy of the numerical results reported below.

The normalized mixed-mode energy release rate and phase angle for the two cases $R_i/R_o = 4/5$ and $R_i/R_o = 2/3$ are plotted in Figs. 8 and 9 respectively, as functions of θ and η. In these figures, the material is taken to be isotropic ($\lambda = \rho = 1$). A remarkable feature of the results for the case of the crack at the center of the beam ($\eta = 1$) is that the relative amount of mode II to mode I increases nearly linearly with the angle θ. The opening mode which dominates for small values of θ shifts steadily towards mode II which is attained at 90°. As the relative amount of mode II to mode I is increased, energy release rate increases sharply, peaks and then decreases gradually to a plateau. Similar trends are observed for cracks lying off the centerline of the beam ($\eta \neq 1$). A crack in the curved beam is clearly going to experience unstable growth under prescribed bending moment if θ is sufficiently small. The growth of larger cracks may be stable or unstable depending on the mode-dependence of the toughness (eqn. (8)). (This is supported by limited experimental evidence showing that fast interlaminar fracture "pops in" at both tips of the pre-crack and arrests at approximately $\theta = 40°$. It has also been reported that secondary cracks then emerge between the first crack and the free surfaces of the specimen.) In the cases of Figs. 8 and 9 for the crack near the top surface of the beam ($\eta = 1/3$), the crack tip becomes pure mode II at a value of θ well below 90° and is closed for larger values of θ. Results have not been presented in this range. For a crack near the lower free surface of the beam ($\eta = 3$), the loading generates a relatively small negative mode II component for small values of θ but the mode II component becomes positive at roughly 10°. The

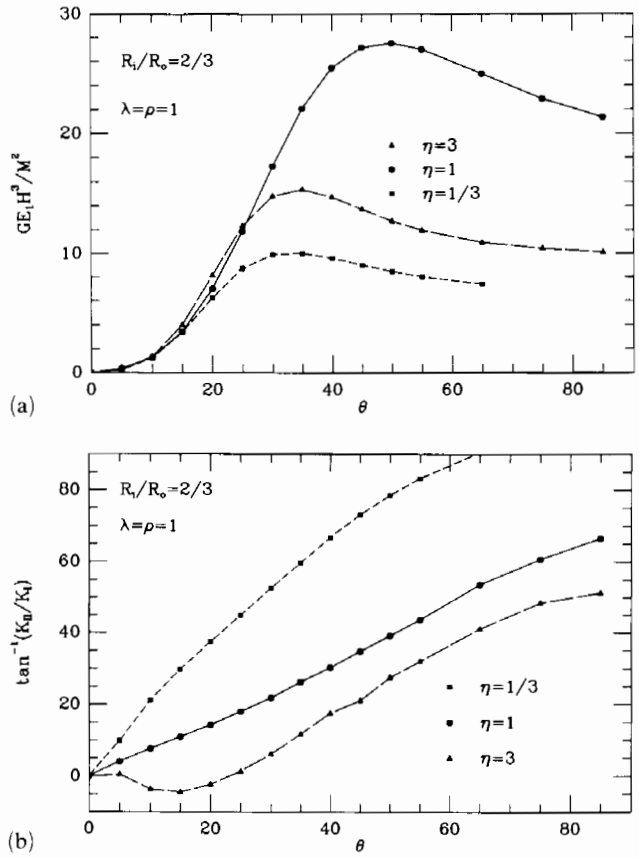

Fig. 9. The η-dependence of (a) energy release rate, and (b) phase angle for $R_i/R_o = 2/3$ and $\lambda = \rho = 1$.

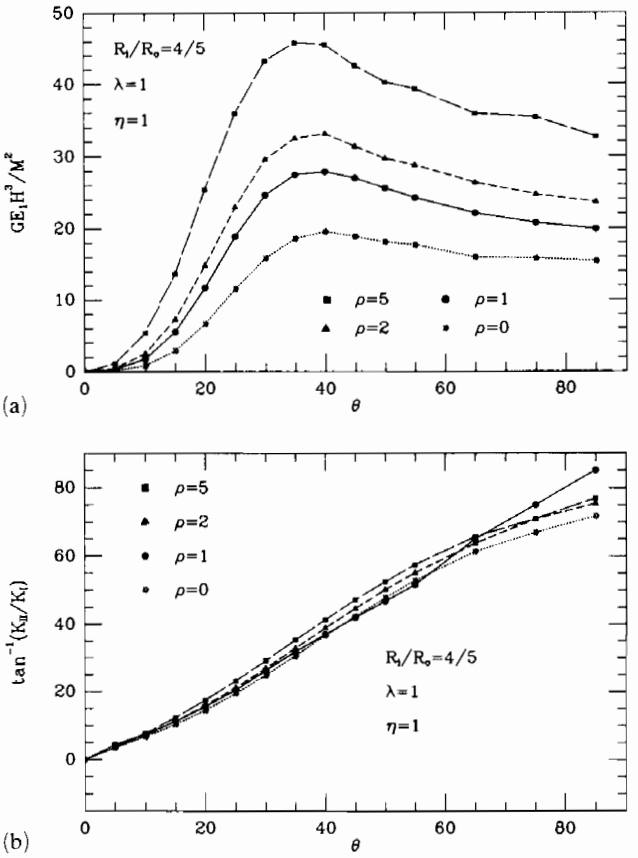

Fig. 10. The ρ-dependence of (a) energy release rate, and (b) phase angle for $R_i/R_o = 4/5$ and $\lambda = \eta = 1$.

trends of the thin beam analysis for the energy release rate fairly faithfully reproduce the results from the finite element calculation. In particular, note that for the thinner of the two curved beams in Fig. 8 the energy release rates for the two cases, $\eta = 1/3$ and 3, which are predicted to be the same by thin beam theory, are indeed close. However, it should also be noted that the phase angle in Figs. 8 and 9 depends very strongly on whether the crack lies inside or outside the center of the beam.

Calculations show that variations of the two dimensionless elasticity parameters ρ and λ affect significantly the level of energy released by the crack, indicating the importance of material anisotropy in accurate characterization of mixed mode delamination fracture. Nearly a twofold increase in G is observed as ρ varies from 0 to 5 (Fig. 10 for $\lambda = \eta = 1$ and $R_i/R_o = 4/5$). Moreover, there is also a very strong influence of the modulus E_2 governing stiffness perpendicular to the beam centerline as can be seen from the λ-dependence of the results in Fig. 11. The dependencies of the energy release rate on the material orthotropy displayed in Figs. 10 and 11 is missed entirely from a thin beam approach. On the other hand, the phase angle of loading is only slightly affected by changes in elasticity parameters λ and ρ, in contrast with the role played by the geometrical parameter η.

5. Conclusions

A numerical study has been conducted to provide relatively complete solutions to two beam delamination problems, a straight beam under transverse load and a curved beam under constant moment. Presentation of results for the problems is complicated by the fact that there are a multitude of geometric and material parameters. The results for the straight beam of orthotropic material are simplified by making use of the orthotropic rescaling technique so that numerical solution to the problem requires three nondimensional variables: a/H, $\eta = h_1/h_2$ and the orthotropy parameter ρ. The curved beam problem depends on five nondimensional parameters. Nevertheless, it has been possible to provide a reasonably complete characterization of the solution. The thin beam theory solution to the curved

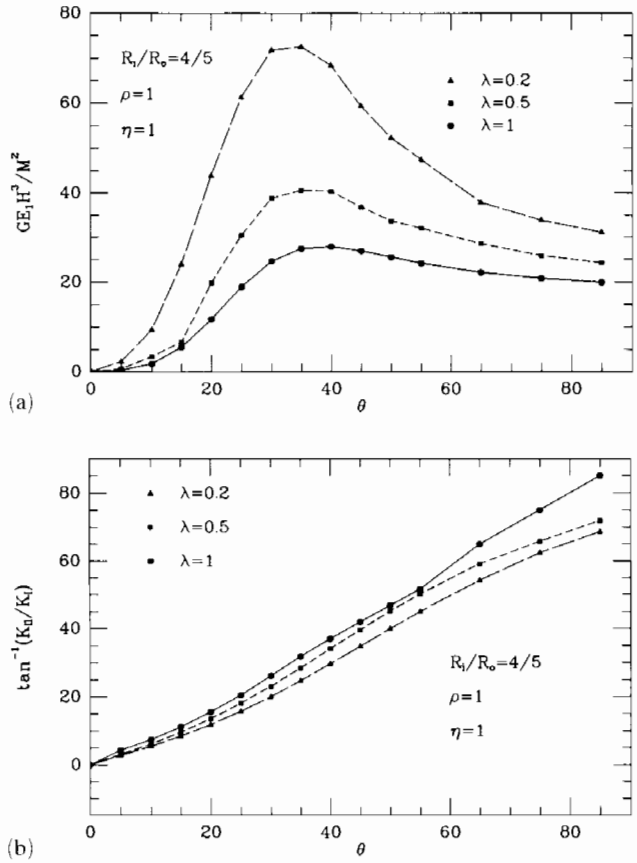

Fig. 11. The λ-dependence of (a) energy release rate, and (b) phase angle for $R_i/R_o = 4/5$ and $\rho = \eta = 1$.

beam problem involves only three parameters, $\eta = h_1/h_2$, a/H and H/R. While this solution loses accuracy for thicker beams, it does capture the main trends of the solution. The results provided in the paper should be useful for the purpose of calibrating specimens and for applications to predict delamination.

Acknowledgments

One of the authors (TJL) wishes to thank Professor J. R. Rice for several helpful discussions. This work was partially supported by DARPA University Research Initiative (Subagreement P.O. #KK3007 with the University of California, Santa Barbara, ONR Prime Contract N00014-92-J-1808), by National Science Foundation (Grant MSS-92-02141) and by the Division of Applied Sciences, Harvard University. Provision of the ABAQUS finite element code by Hibbitt, Karlsson and Sorensen, Inc. of Providence, RI is gratefully acknowledged.

References

1 Z. Suo, *J. Appl. Mech.*, *57* (1990) 627–634.
2 G. C. Sih, P. C. Paris and G. R. Irwin, *Int. J. Fract.*, *1* (1965) 189–203.
3 A. J. Kinloch, *Adhesion and Adhesives*, Chapman and Hall, London, 1987.
4 H. C. Cao and A. G. Evans, *Mech. Mater.*, *7* (1989) 295–305.
5 K. M. Liechti and Y.-S. Chai, *J. Appl. Mech.*, *59* (1992) 295–304.
6 J. Ahmad, *J. Eng. Mater. Technol.*, *115* (1993) 101–105.
7 S. G. Lekhnitskii, *Theory of Elasticity of an Anisotropic Body*. Mir Publishers, Moscow, 1981.
8 W. B. Fichter, *Stresses at the Tip of a Longitudinal Crack in a Plate Strip*, NASA Technical Report TR-R-265, 1967.
9 H. Tada, P. C. Paris and G. R. Irwin, *The Stress Analysis of Cracks Handbook*, Del Research, St. Louis, MO, 1985.
10 A. J. Russell and K. N. Street, Moisture and temperature effects on the mixed-mode delamination fracture of unidirectional graphite/epoxy, in *Delamination and Debonding of Materials, ASTM STP 876*, 1985, pp. 349–370.
11 J. G. Williams, *Int. J. Fract.*, *36* (1988) 101–119.
12 S. Timoshenko and J. M. Lessells, *Applied Elasticity*, Constable, London, 1928.

Appendix A: Pure bending of a curved beam with cylindrical anisotropy

The problem to be solved is that of the uncracked beam in Fig. 2(b). The notation used in this Appendix is shown in Fig. A(1). In polar coordinates, the equations of equilibrium are satisfied by introducing a stress function $\phi(r, \theta)$ such that

$$\sigma_r = \frac{1}{r}\frac{\partial \phi}{\partial r} + \frac{1}{r^2}\frac{\partial^2 \phi}{\partial \theta^2}$$

$$\sigma_\theta = \frac{\partial^2 \phi}{\partial r^2} \qquad \text{(A1)}$$

$$\tau_{r\theta} = -\frac{\partial}{\partial r}\left(\frac{1}{r}\frac{\partial \phi}{\partial \theta}\right)$$

For the pure bending problem in consideration, the distribution of stress components does not depend on θ and, in addition, $\tau_{r\theta} \equiv 0$. For the cylindrical material anisotropy, the equation of compatibility simplifies to

$$\frac{d^4\phi}{dr^4} + \frac{2}{r}\frac{d^3\phi}{dr^3} - \frac{\lambda}{r^2}\frac{d^2\phi}{dr^2} + \frac{\lambda}{r^3}\frac{d\phi}{dr} = 0 \qquad \text{(A-2)}$$

which is independent of ρ. The general solution to this ordinary differential equation is

$$\phi = c_1 + c_2 r^2 + c_3 r^{1+\sqrt{\lambda}} + c_4 r^{1-\sqrt{\lambda}} \qquad \text{(A-3)}$$

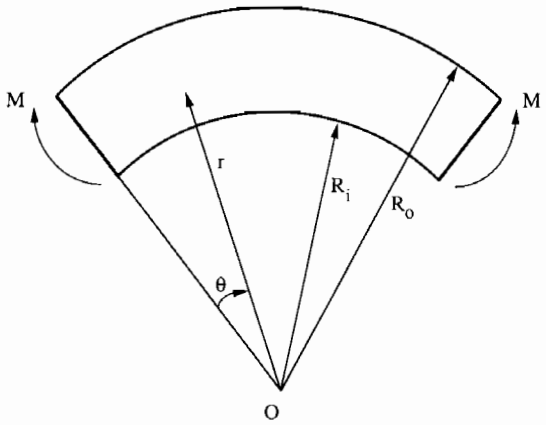

Fig. A1. Pure bending of a curved beam with cylindrical anisotropy.

from which

$$\sigma_r = 2c_2 + (1+\sqrt{\lambda})c_3 r^{\sqrt{\lambda}-1} + (1-\sqrt{\lambda})c_3 r^{-\sqrt{\lambda}-1}$$
$$\sigma_\theta = 2c_2 + (1+\sqrt{\lambda})c_3 r^{\sqrt{\lambda}-1} - (1-\sqrt{\lambda})c_3 r^{-\sqrt{\lambda}-1} \quad \text{(A-4)}$$

The boundary conditions are

$$\sigma_r = 0 \quad \text{for} \quad r = R_o \quad \text{and} \quad r = R_i$$
$$\int_{R_i}^{R_o} \sigma_\theta \, dr = 0, \qquad \int_{R_i}^{R_o} \sigma_\theta \, r \, dr = -M \quad \text{(A-5)}$$

The constants c_2, c_3, c_4 are readily obtained from the boundary conditions. The final result for σ_r is

$$\sigma_r = \frac{2M}{AR_i^2}\left[(\zeta^{1+\sqrt{\lambda}} - \zeta^{1-\sqrt{\lambda}}) - (\zeta^{1+\sqrt{\lambda}} - 1)\left(\frac{R_i}{r}\right)^{1-\sqrt{\lambda}} + (\zeta^{1-\sqrt{\lambda}} - 1)\left(\frac{R_i}{r}\right)^{1+\sqrt{\lambda}}\right] \quad \text{(A-6)}$$

where $\zeta = R_i/R_o$ and

$$A = \frac{1-\sqrt{\lambda}}{1+\sqrt{\lambda}}\frac{(\zeta^{1+\sqrt{\lambda}}-1)^2}{\zeta^{1+\sqrt{\lambda}}} + \frac{1+\sqrt{\lambda}}{1-\sqrt{\lambda}}\frac{(\zeta^{1-\sqrt{\lambda}}-1)^2}{\zeta^{1-\sqrt{\lambda}}}$$

For the transverse isotropic material ($\lambda = \rho = 1$), the solution for σ_r has the limit given in ref. A1:

$$\sigma_r = -\frac{4M}{A'}\left(-\frac{R_o^2 R_i^2}{r^2}\ln\zeta + R_o^2 \ln\frac{r}{R_o} + R_i^2 \ln\frac{R_i}{r}\right) \quad \text{(A-7)}$$

with

$$A' = R_o^4(1-\zeta^2)^2 - 4R_o^2 R_i^2 (\ln\zeta)^2$$

Reference

A1 S. Timoshenko and J. N. Goodier, *Theory of Elasticity*, McGraw-Hill, New York, 1951.